Mixing mechanisms in a low-sheared inhomogeneous bubble column

Elise Alméras, Cécile Plais, Véronique Roig, Frédéric Risso, Frédéric Augier

Mixing mechanisms in a low-sheared inhomogeneous bubble column

Elise Alméras [a,b,*], Cécile Plais [b], Véronique Roig [a], Frédéric Risso [a], Frédéric Augier [b]

[a] Institut de Mécanique des Fluides de Toulouse (IMFT), Université de Toulouse, CNRS, INPT, UPS, Toulouse, France
[b] IFP Energies nouvelles, Rond-point de l'échangeur de Solaize, BP 3, 69360 Solaize, France

HIGHLIGHTS

- We study the mixing of a passive scalar in a low sheared bubble column.
- The dye is advected by the recirculation and diffuses due to the bubbles agitation.
- Shear induced turbulence should be accounted for in more heterogeneous cases.

Keywords:
Bubble column
Mixing
Bubble-induced agitation
Buoyancy-driven flow

ABSTRACT

This paper reports an experimental study of the mixing of a passive scalar in a bubble column at high Reynolds number and average gas volume fractions ranging from 2.0% to 7.5%. Starting from a homogeneous bubble column, the bubbly flow is progressively destabilized by imposing a gradient of gas volume fraction at the bottom of the tank. In that way, a single recirculation is produced, which allows to investigate the impact of a large scale buoyancy driven flow on the mixing of a passive scalar. It is shown that, as long as the shear induced turbulence generated by the recirculation is negligible, mixing results from two main mixing mechanisms: the transport by the mean liquid velocity and the mixing induced by the bubbles. While the transport by the liquid recirculation can be accounted for by an advection term, the mixing induced by the bubbles is a diffusive process, the effective diffusivity of which has been measured in a homogeneous bubble column by Alméras et al. (2015). However, once the shear induced turbulence produced by the shear develops, its role upon the mixing has to be taken into account too.

1. Introduction

Bubble columns are commonly used in various industrial fields such as chemical processes, bioengineering, refining and water treatment. One main reason for this keen interest is due to the fact that good mixing and transfer efficiency are achieved without the need of any additional mechanical stirring. However, predicting mixing in bubbly flows is still challenging, mainly because of the existence of various flow regimes that depend on the column size and the gas flow rate (Kantarcia et al., 2004; Chen et al., 1994). In particular, at low gas flow rate, the bubbly flow remains stable; that is the so called homogeneous regime. A series of experimental investigations carried out in homogeneous columns have led to a rather complete description of the properties of the turbulence induced by bubbles (Martínez Mercado et al., 2007, 2010; Riboux et al., 2010; Mendez Diaz et al., 2013). It appears that the agitation induced by bubbles strongly differs from the turbulence induced by the shear and it results mainly from two contributions: the flow disturbances generated in the vicinity of the bubbles and the turbulence resulting from the instability of the flow through the population of bubbles.

When the gas flow rate is increased, the heterogeneous regime is achieved, leading to a reorganization of the flow. It is characterized by the presence of a transverse gas volume fraction gradient and the development of large scale buoyancy driven motions (Chaumat et al., 2006; Degaleesan et al., 2001). As the inhomogeneity is increased, shear induced turbulence is produced and develops on a wider and wider range of length scales (Maximiano, 2015). The resulting hydrodynamics properties of the flow involve thus a large range of length scales, from length scales which are smaller than the bubble diameter up to the column diameter. Due to the complexity of the flow structure, it is still challenging to predict the mixing of a passive scalar in such a flow regim. In the most general case, the mixing of a passive scalar in a heterogeneous bubble column thus results in the combination of three different contributions: (1) the transport by the buoyancy driven recirculations at the scale of the bubble column, (2) the mixing by the bubble induced agitation at scales around

* Corresponding author at: Laboratoire de Génie Chimique (LGC), Université de Toulouse, CNRS, INPT, UPS, Toulouse, France.
E-mail address: elise.almeras@ensiacet.fr (E. Alméras).

https://doi.org/10.1016/j.ces.2018.04.026

the bubble diameter, and (3) the mixing by the shear induced tur bulence on a wide range of scales from the scale of the column to scales smaller than the bubbles. Each mixing mechanism requires a specific modeling, which is relatively well understood when it is considered independently of the two others. (1) The transport by the large scales can be simply described by the advection by the mean velocity of the liquid phase. (2) The mixing induced by bub bles has been shown to be a diffusive process that can be modeled by two effective diffusivity coefficients, D_v for the vertical direction and D_h for the horizontal direction (Mareuge and Lance, 1995; Abbas et al., 2009; Alméras et al., 2015; Loisy, 2016). According to Alméras et al. (2015), the two diffusion coefficients are increas ing functions of the gas volume fraction α, such that $D_v > D_h$. Two regimes must be distinguished. At low gas volume fraction, the dif fusion coefficients evolve as the square root of α, whereas they tend towards a constant value at larger α. (3) The mixing by the shear induced turbulence in a single phase flow can be modeled by an effective turbulent diffusivity coefficient, $D_t \quad \nu_t/S_{ct}$, that can be deduced from the effective turbulent viscosity ν_t by assum ing a value of the turbulent Schmidt number close to 1 (Combest et al., 2011). Even though the model of each mixing mechanism is rather well understood when it is considered in the absence of the others, mixing in a heterogeneous bubble column remains poorly understood since it results from the interaction of these three contributions.

Our strategy to gain knowledge on this topic consists in study ing different flow configurations where the relative weight of each contribution is varied. Previously in Alméras et al. (2016), we stud ied, both numerically and experimentally, the mixing of a passive scalar in an heterogeneous bubbly flow where the mixing by shear induced turbulence and bubble induced agitation were of the same order. It turned out that summing the effective diffusiv ities of the two contributions ($D_{total\ i} \quad D_t + D_i$, where $i \quad h$ or v rep resents respectively the horizontal and vertical direction) led to a good prediction of the mixing time. The present work focuses on a heterogeneous bubbly flows where the mixing by bubble induced agitation is combined with a two dimensional large scale recirculation, but where shear induced turbulence is negligi ble. To ensure the two dimensional aspect of the flow, we operate a rectangular bubble column and develop a novel gas injection sys tem that allows to impose a well controlled gradient of gas volume fraction at the bottom of the column. One advantage of this config uration is that the gradient of gas volume fraction in the column can be controlled independently from the global gas volume frac tion. By increasing progressively the gradient of gas volume frac tion, the flow is progressively destabilized, allowing the shear induced turbulence to develop on a wide range of length scales. In this work, we consider only weak gradients so that the contribu tion of the turbulence induced by the shear is negligible and the liquid recirculation remains two dimensional. This experimental set up allows thus the investigation of the impact of a large scale recirculation on the mixing time in a bubble column and could be use to validate CFD models.

The paper is organized as follows. In Section 2, the experimental set up and the different flow configurations are presented. In Sec tion 3, the procedure for mixing experiments and the measure ment techniques are introduced. Mixing mechanisms are then described and discussed in Section 4 for each flow configuration and concluding remarks are given in Section 5.

2. Experimental set-up and flow configurations

The experimental set up is depicted in Fig. 1. It is a rectangular bubble column, made of an open tank of 1000 mm height with a cross section of 300×150 mm^2. The tank is filled with tap water over a height $H \quad 800$ mm. Bubbles with a diameter $d = 3$ mm are generated at the bottom of the tank using 1800 capillary tubes of 0.2 mm diameter disposed in a regular array with a space step of 0.5 mm. The capillary tubes are supplied with gas by two separated pressurized chambers. Both chambers can be connected (resp. dis connected) through a valve opening (resp. closure). This gas injec tion system allows to generate two kinds of flow. When the valve is open, the pressure in each chamber is identical and a homoge neous bubbly flow is generated, with a zero mean liquid velocity everywhere within the column. The average gas volume fraction over the column $\langle\alpha\rangle_t$ is adjusted by varying the total gas flow rate Q_g . We checked that in this mode, the flow remains homogenous up to $\langle\alpha\rangle_t \quad 15\%$ since the gas volume fraction evolves linearly with the superficial gas velocity $J_g \quad Q_g \times S$, where S is the cross section surface (Fig. 2). On the other hand, when the valve is closed, the gas pressure in the two chambers differs, leading to the gener ation of a gradient of gas volume fraction at the bottom of the tank in the horizontal x direction. Introducing such a gradient at the gas inlet allows thus the production of a heterogeneous flow at low gas flow rate. In fact, large scale recirculations are produced due to buoyancy effect. In this configuration, two operating parameters need to be settled: the global gas volume fraction $\langle\alpha\rangle_t$ and the dif ference of gas volume fraction $\Delta\alpha$ which is imposed at the bottom of the tank. Both parameters are adjusted separatetly by varying the gas flow rate in the upstream section and the pressure differ ence between the two chambers. Depending on these two operat ing parameters, various flow structures can be produced, such as steady or unsteady flows, and two dimensional or three dimensional recirculations. In order to generate a study two dimensional recirculation in the $(x;z)$ plane, we considered only weak gas volume fraction differences ($\Delta\alpha \leqslant 0.4\langle\alpha\rangle_t$) and we lower the level of water to 600 mm above the bubble injection.

Two classes of flows are investigated in the following paper. The first one corresponds to a homogeneous bubbly flow, where no large scale recirculation is present. It includes two configurations, called H1 and H2, corresponding to an average gas volume fraction $\langle\alpha\rangle_t \quad 4.5\%$ and $\langle\alpha\rangle_t \quad 7.0\%$, respectively (Table 1). The second class of flows comprises three configurations, named I1, I2 and I3, all with a single large scale recirculation but different $\Delta\alpha$ (Table 1).

The properties of the gas phase are characterised for both classes of flow by using a dual optical fiber probe from RBI, which allows the determination of the local gas volume fraction α and the bubble rising velocity V (see Riboux et al., 2010; Colombet et al., 2014 for details about the measurement techniques). The optical fiber is 5 mm diameter with a very thin tip which ensures a good piercing of the bubbles. The probe holder is 1 cm diameter, which is small enough not to disturb the flow in the column significantly. Fig. 3 presents horizontal profiles of α and V, at different elevations z for a given depth position ($y \quad 7.5$ cm). For homogeneous bubbly flows, we checked that the gas volume fraction and bubble rise velocity remain uniform along the x direction for all average gas volume fractions from $\langle\alpha\rangle_t \quad 3.1\%$ to $\langle\alpha\rangle_t \quad 7.0\%$ (Fig. 3 (a) & (b)). A slight gradient of bubble velocity, lower than 0.05 s ^{1}, is observed at the higher gas volume fraction, probably due to a slight tilt of the bubble column. The corresponding velocity difference, which is equal to 1.2 cm/s, is however negligible compared with the bubble rise velocity. More informations about the dynamics of the homogenous bubble swarm can be found in Riboux et al. (2010) and Colombet et al. (2014), where the mean bubble rise velocity and the drag coefficient are reported as a function of the gas volume fraction. On the other hand, strong horizontal gradients of gas volume fraction and bubble rising velocity are present at all the vertical positions in configurations I1 2. In particular, $\Delta\alpha$ at $z \quad 10$ cm is equal to 0.5% in configuration I1 and 1.4% in config

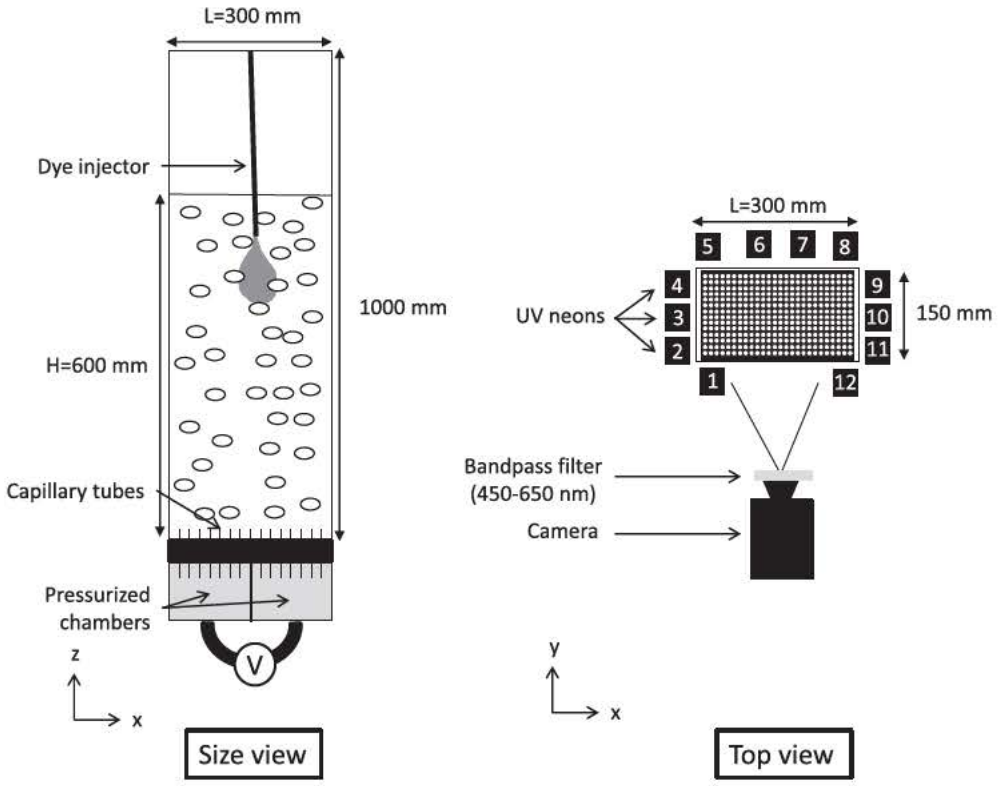

Fig. 1. Experimental set-up.

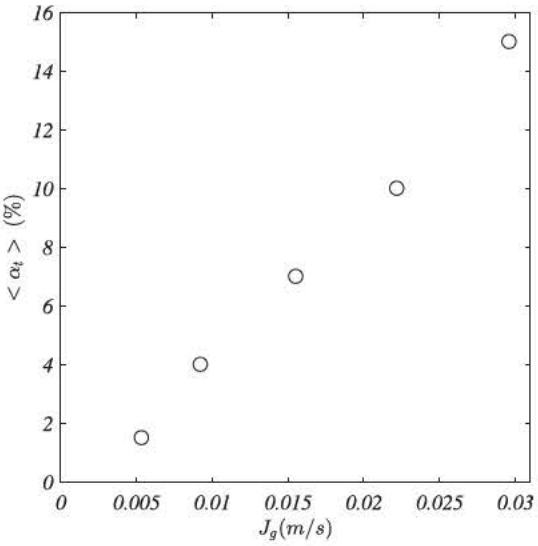

Fig. 2. Gas volume fraction average over the column $\langle\alpha\rangle_t$ as a function of the superficial gas velocity J_g in the homogeneous regime.

uration I2. Then, at higher vertical positions, the gradient of gas volume fraction decreases. The imposed gas volume fraction gradient produces a mean liquid recirculation in the column, the average liquid velocity being positive (resp. negative) in the region where the gas volume fraction is larger (resp. lower). This leads to consider two distinct areas in the flow, namely: an upstream leg on the right hand side where the liquid velocity is positive, and a downstream leg on the left hand side where the velocity is negative. Due to the presence of the recirculation, bubbles are accelerated in the upstream leg and slowed down in the downstream leg. Figs. 3 (d) & (f) illustrate such an effect, where the maximal bubble rise velocity reaches 37 cm/s at y 23.4 cm in configuration I1 and 44 cm/s at y 30 cm in configuration I2. Note that the horizontal gradient of the bubble rising velocity tends to decrease for $z > 40$ cm.

Five quantitative parameters are defined to characterize the flow configurations. The first two parameters concerns the gas volume fraction in the column. Especially, one parameter is the global gas volume fraction $\langle\alpha\rangle_t$, which is measured by averaging optical probe measurements all over the tank. The other is the gas volume fraction difference $\Delta\alpha$ at the bottom of the tank, which is determined from the difference between the maximum and the minimum values of the gas volume fraction over the horizontal profile at z 10 cm.

We then estimate the superficial gas velocities of the two legs since they are supplied with a different gas flow rate. As we did not measure directly the gas flow rate in each leg, we deduce the superficial gas velocity from the bubble rising velocity and gas volume fraction (J_g $\alpha \times V_b$) at z 10 cm. We then average J_g in the horizontal direction over x [15; 0] cm (resp. x [0; 15] cm) in order to estimate the superficial gas velocity in the left side of the gas injector (resp. right side).

The last hydrodynamic parameter we consider is the characteristic scale U of the mean liquid recirculation velocity. Assuming that the bubble velocity V_r relative to the liquid is identical everywhere in the column, the mean liquid recirculation can be estimated by means of the bubble rise velocity difference between the upstream and downstream legs. The bubble velocity being expressed as $V(x;z)$ $V_r + u(x;z)$, where u is the local liquid velocity, we determine $\langle V_z\rangle(x)$ as the vertical bubble velocity at location x averaged in the vertical direction over the range z 10.7 29.2 cm for configuration I1 and z 9.6 40.6 cm for configuration I2. The profiles of $\langle V_z\rangle(x)$ are shown in Figs. 3 (d) & (f) by thick black lines. The characteristic liquid recirculation velocity U is then calculated by considering the maximum and the minimum of these profiles: U $\{max[\langle V_z\rangle]$ $min[\langle V_z\rangle]\}/2$.

Table 1
Hydrodynamic and mixing properties of the four configurations. $\langle\alpha\rangle_t$: Mean gas volume fraction averaged over the tank. $\Delta\alpha$: Gas volume fraction difference imposed at the bottom of the tank. J_{gd}: Superficial velocity in the downstream section. J_{gu}: Superficial velocity in the upstream section. U: Liquid recirculation velocity. V_p: Propagation velocity of the concentration field. T_m: Experimental mixing time.

	Hydrodynamic properties					Mixing properties	
	$\langle\alpha\rangle_t$ %	$\Delta\alpha$ %	J_{gd} cm/s	J_{gu} cm/s	U cm/s	V_p cm/s	T_m s
Configuration H1	4.5	0	0.9	0.9	0	0	139.3 ± 20
Configuration H2	7.0	0	1.5	1.5	0	0	126.5 ± 18
Configuration I1	2.0	0.5	4.2	6.9	5.4	6.6 ± 0.8	30.5 ± 0.6
Configuration I2	3.5	1.4	6.2	11.9	11.1	12.2 ± 1.0	21.5 ± 0.9
Configuration I3	3.5	>1.4	–	–	–	14.5 ± 0.7	14.5 ± 0.9

Table 1 lists the hydrodynamic parameters for the five investi gated configurations. Note that no optical fiber probe measure ment is available in case I3, so that $\Delta\alpha$ and U are unknown. However, we know that $\langle\alpha\rangle_t$ 3.5% and $\Delta\alpha > 1.4\%$ from the inlet gas flow rate and we will show later that the liquid recirculation velocity can be deduced from the mixing experiments by measur ing the dye propagation velocity V_p.

We can anticipate from Table 1 that the chosen flow configura tions are contrasted. Configurations H1 2 corresponds to homoge neous bubbly flows without any large scale recirculations. They will be used as reference cases where the mixing is only due to bubble induced agitation. In configurations I1 2, the moderate gra dient of gas volume fraction is responsible for a significant large scale recirculation loop but does not generate any significant shear induced turbulence. In this case, the mixing is controlled by the buoyancy induced mean motion at the scale of the column and by bubble induced agitation at the scale of the bubbles. In case I3, buoyancy driven fluctuations in the same range of scales as the bubble induced agitation develop.

3. Mixing experiments and instrumentation

Two types of mixing experiments have been carried out. The main experiments were based on local measurements of the con centration of a fluorescent dye and allowed the determination of mixing times in various regions of the column. In addition, sec ondary experiments were based on the so called *colorimetric tech nique* and were used to determine the mixing time in the whole column in the case of homogeneous flows.

Let us first describe the main experimental procedure. Mixing experiment are carried out by injecting a solution of fluorescein sodium within the bubble swarm. It is a fluorescent dye with a low molecular diffusivity D_m, which is characterized by a high Sch midt number: S_c $\nu/D_m \approx 2000$. A volume of 1 mL of the dye solu tion, at concentration 5×10^{-3} mol/L, is injected during 2 s through a vertical tube (0.5 mm inner diameter and 0.9 mm outer diame ter) by means of a syringe pump. In homogeneous cases H1 2, the tip of the dye injector is located in the middle of the tank in a horizontal plane located at 500 mm above the bubble injection (see Fig. 4). In inhomogeneous cases I1 3, the dye injector is moved to various locations (indicated by circles in Figs. 5 7), in order to explore the downstream and upstream legs of the liquid recirculation.

The lighting is provided by 12 UV neon tubes disposed around the tank (Fig. 1). The neon light wavelength ranges from 300 to 440 nm, ensuring a significant fluorescence of the dye in the range of wavelengths from 450 650 nm. The fluoresced light emitted by the dye is recorded at a frequency of 49 Hz by a camera PCO EDGE sCMOS (2560×2160 pixels, 16 bits) equipped with a 85 mm optical lens with an aperture f/D 2.8 for the configuration H1 2 and f/D 2 for the configuration I1 3. An optical bandpass filter (450 650 nm) is mounted in front of the lens in order to film only the fluoresced light. We checked that the depth of field is larger than the test section and the variation of magnification throughout the imaged volume of the flow is negligible. The dimensions of the field of view are 280×370 mm for cases H1 2 and 493 × 188 mm for cases I1 3. In that way, the dispersion of the dye is observed over the whole flow during 40 s. Before one can analyse the mixing, the raw images need to be processed in order to deal with optical disturbances induced by the bubbles, such as reflexions, refractions and occultations of the fluoresced light by the bubble interfaces. We used here the image processing developed by Alméras et al. (2015), which was proved to be valid for measuring concentration field in a homogeneous bubble columns. In the present study, the gas volume fraction gradient remains small enough to justify the use of the same image processing.

Figs. 4 7 present typical dye distribution obtained after image processing, for the configurations H1, I1, I2 and I3, respectively. Experiments have been repeated five times per each configuration and injection position, except for configuration I3, where only two runs per injection point were performed. No dependence of the mixing times upon the injection position was observed, so that averaging could be performed over 5 runs for configurations H1 2, 15 runs for configurations I1 2, and 6 runs for configuration I3.

Additional mixing experiments have been performed by means of the colorimetric method, which is commonly used in chemical engineering to measure the overall mixing time T_m, which is the time required to get a homogeneous concentration over the whole column (Pandit and Joshi, 1983; McClure et al., 2015). A dye, Purple Drimarene (R2RL, Clariants), is injected into the middle of the col umn by means of a dye injector tube similar to Gabelle et al. (2011) and Plais and Augier (2016). A camera images the dispersion of the dye over the whole column at a frame rate of 25 Hz, during a time period of at least 150 s. Mixing times are then calculated by means of an in house image processing software. A full description of it can be found in Plais and Augier (2016). A qualitative comparison between the local mixing of the fluorescent dye (over 15 s) and the global mixing of Purple Drimarene (over 60 s) is shown in Fig. 4 for configuration H1. The two methods allow to visualise the spread ing of the dye distribution in both the vertical and the horizontal direction. In particular, the propagation speed of the front of the dye distribution determined by the two techniques is the same. We can therefore conclude that the two techniques are reliable to measure mixing times.

4. Transport and mixing mechanisms

Figs. 4 7 show the dye distribution at different instants for a mixing experiment for each configuration H1, I1, I2 and I3. At a glance, we see that the mixing strongly differs depending on the flow regime. In the homogeneous case (configurations H1 2, Fig. 4), the dye distribution spreads over time in both the horizon tal and vertical directions, but does not experience any large scale motions. The center of mass of the dye distribution, which is mate

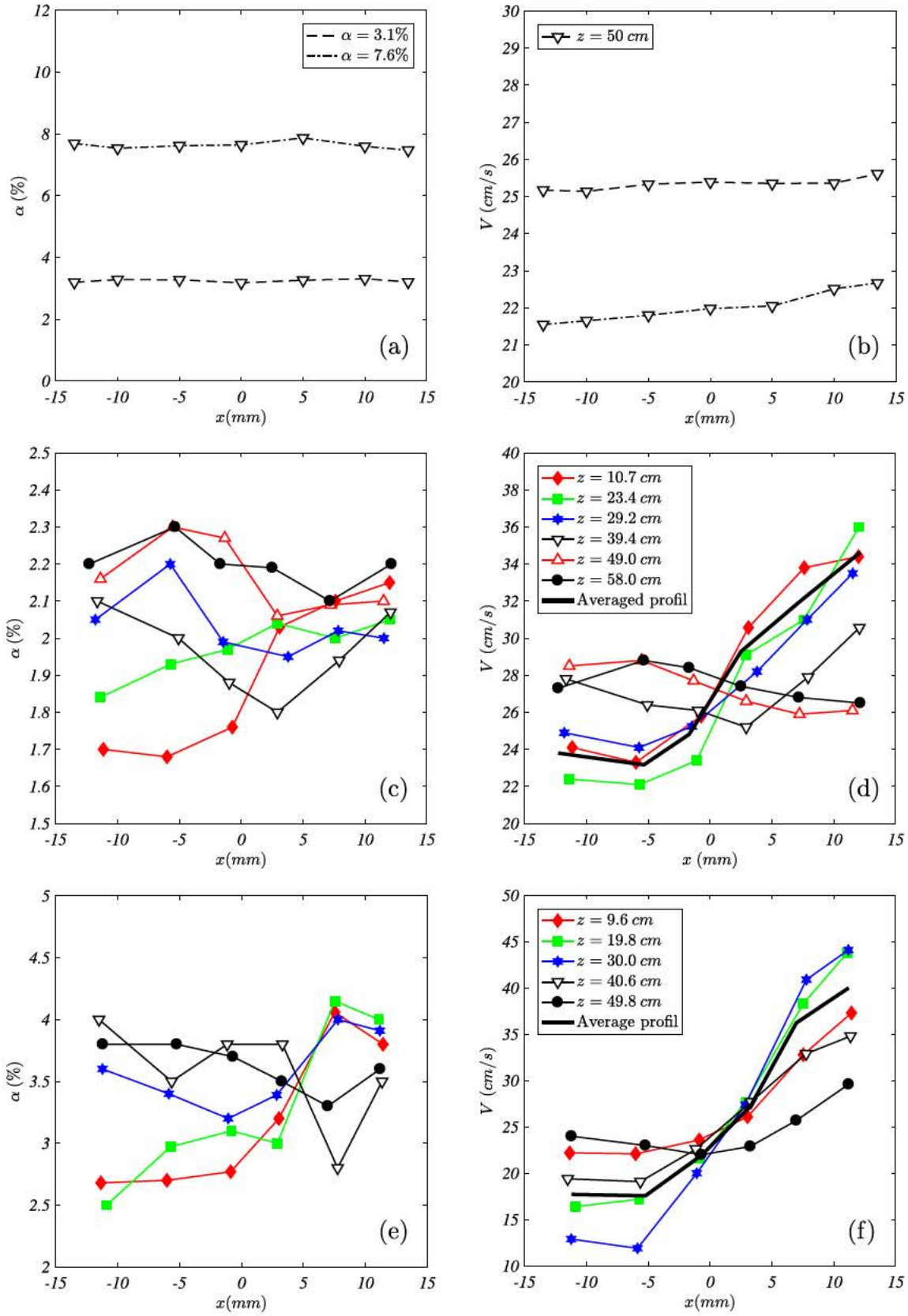

Fig. 3. Horizontal profiles of the gas volume fraction (to the left) and of the bubble velocity (to the right) at different elevations z. (a)-(b): Homogeneous bubbly flows H1-2. (c)-(d): Configuration I1. (e)-(f): Configuration I2.

rialized by a green cross in Fig. 4 *top*, remains almost at the same location. Mixing results solely from the bubble induced agitation, which mainly involves fluctuations at the bubble scale. In this case, the mixing can be well described by a regular diffusive process characterised by two effective diffusion coefficients D_h and D_v (Alméras et al., 2015). The process is rather slow and leads to an

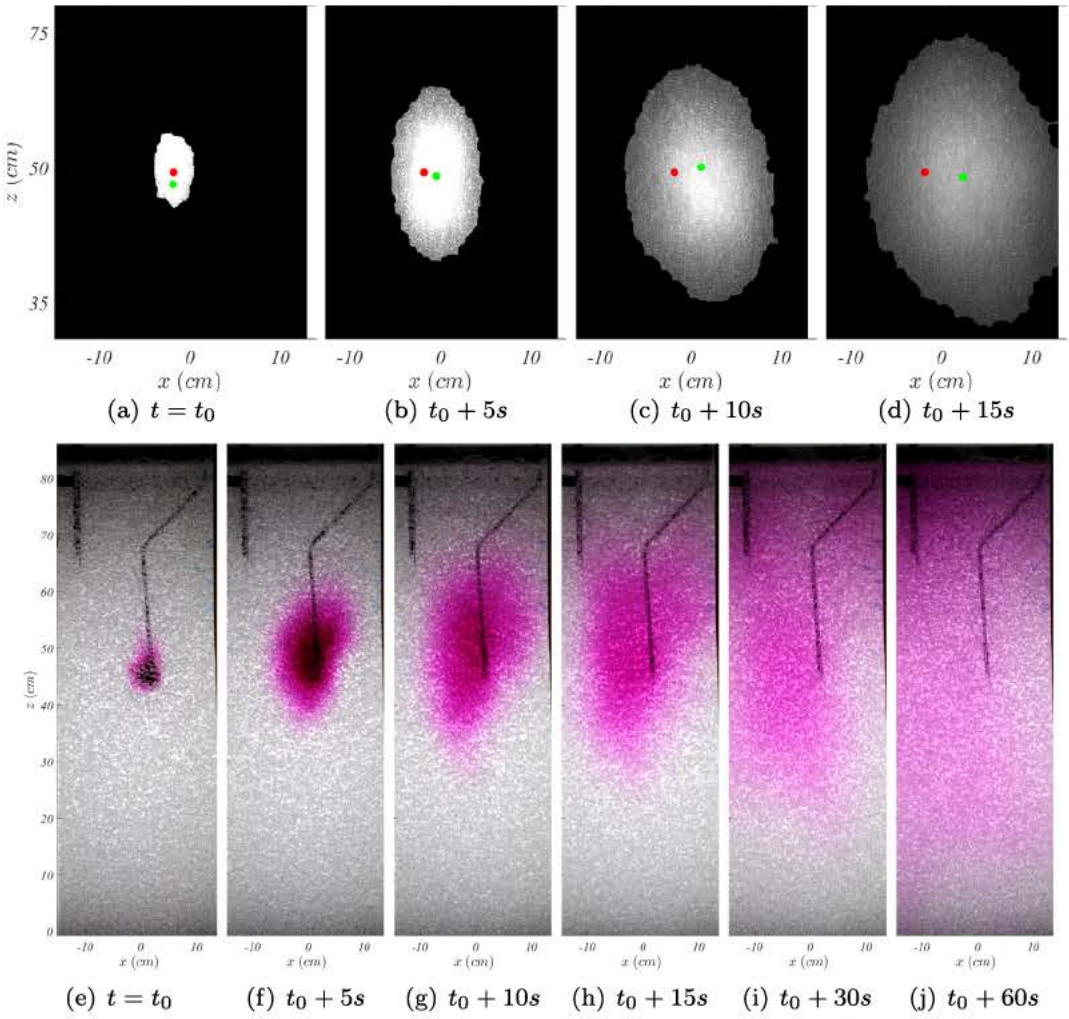

Fig. 4. Pictures of the mixing process in configuration H1 visualised by fluorescence induced by UV light ((a)–d)) and by colorimetry ((e)–j)). The dye injection is stopped at t t_0. The red circles represent the location of the dye injection. The green circles represent the center of mass of the dye distribution. (For interpretation of the references to colour in this figure legend, the reader is referred to the web version of this article.)

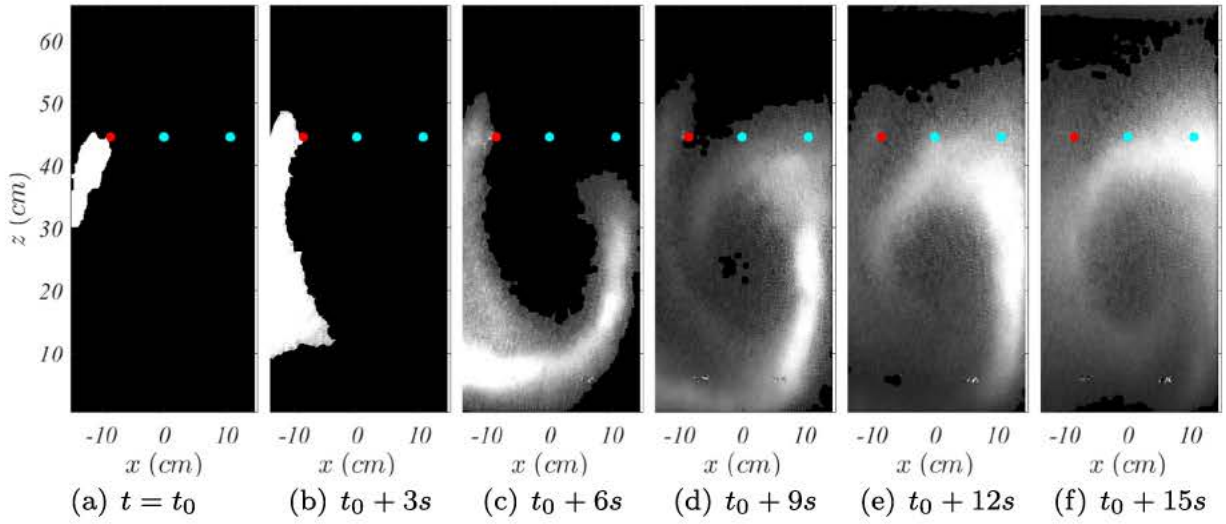

Fig. 5. Pictures of the mixing process in configuration I1. The dye injection is stopped at t t_0. The red circle represents the injection point of the dye in the present example. The cyan circles represent the other injection points. (For interpretation of the references to colour in this figure legend, the reader is referred to the web version of this article.)

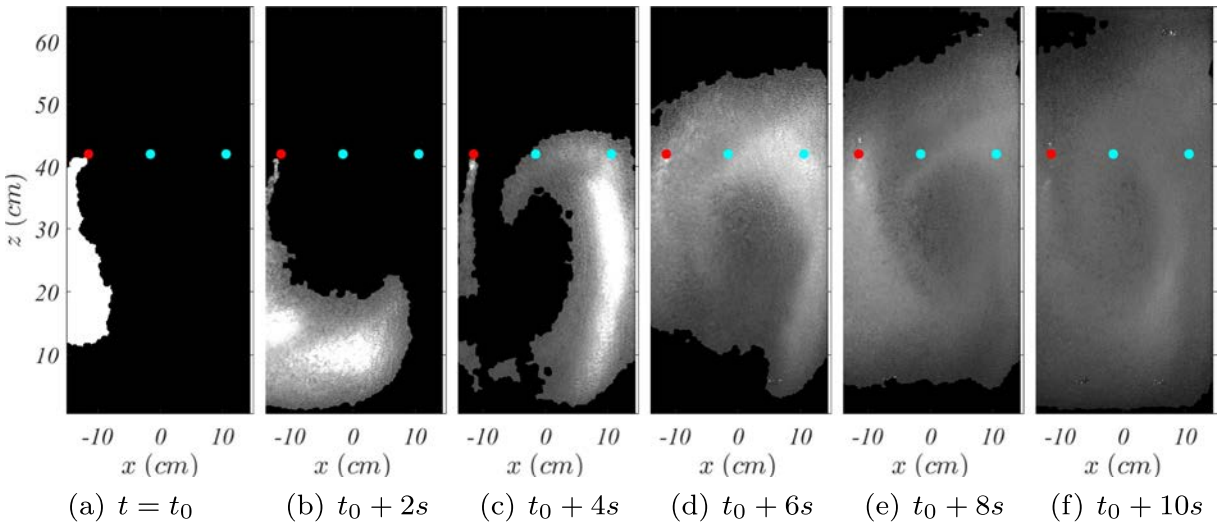

Fig. 6. Pictures of the mixing process in configuration I2. The dye injection is stopped at t t_0. The red circle represents the injection point of the dye in the present example. The cyan circles represent the other injection points. (For interpretation of the references to colour in this figure legend, the reader is referred to the web version of this article.)

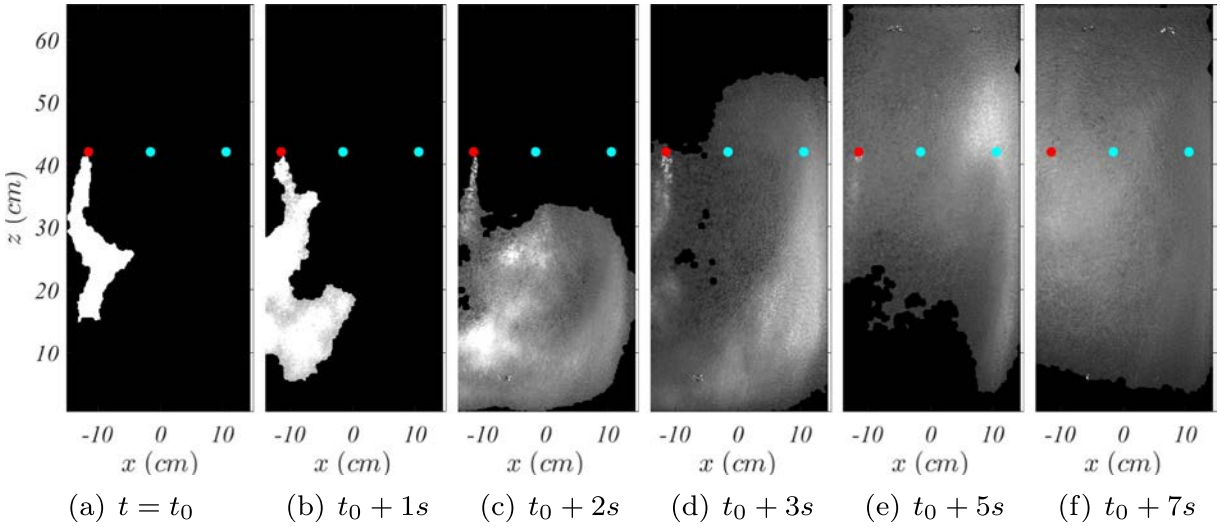

Fig. 7. Pictures of the mixing process in configuration I3. The dye injection is stopped at t t_0. The red circle represents the injection point of the dye in the present example. The cyan circles represent the other injection points. (For interpretation of the references to colour in this figure legend, the reader is referred to the web version of this article.)

overall mixing time larger than 120 s at $\langle \alpha \rangle_t$ 7% (Table 1). In con trast, when a recirculation is present (configurations I1 3), the dye distribution is rapidly transported over the height of the column, leading to a significantly shorter mixing time. The dye distribution takes approximately 10 s to go through the column in case I1 and 5 s in cases I2 3. However, the penetration of the dye in the heart of the recirculation requires a longer time since concentration inho mogeneities are observed until 15 s in case I1 and 7 s in cases I2 3. The diffusion in the horizontal direction is therefore the lim iting mechanism which controls the mixing time.

In order to get more insight, two quantitative parameters are introduced to describe mixing in the inhomogeneous case: *(i)* a propagation velocity V_p that characterizes the global motion of the dye distribution and *(ii)* the mixing time T_m. These two param eters are measured as follows. The visualisation field is decom posed in 5 boxes, which are defined in Fig. 8(a). Box 1 is located in the downstream region, box 3 in the upstream one, box 2 at the bottom of the column, box 4 at the top and box 5 in the middle of the recirculation. The flow within boxes 1 to 4 is subject to a strong advection whereas the mean velocity is almost zero in box 5. The grey levels in the images of the fluorescent dye are pro portional to the concentration. We can thus characterize the mix ing process by considering the average $\langle F \rangle_b$ of the grey levels over each box b. Fig. 8(b) presents a typical time evolution in case I2 of the values of $\langle F \rangle_b$, which have been normalized by the final level $\langle F \rangle_{b\infty}$ that is reached when the mixing is completed.

In the regions subjected to advection (boxes 1 4), the average grey level presents oscillations which are damped over time. The maximum amplitudes are the signature of the successive passages of the dye patch, whereas the damping of the oscillations is that of mixing. The successive instants t_p when maximum amplitudes are reached in boxes 1 4 are marked by black crosses in Fig. 8(b). The instants t_p can then be used to determine the propagation velocity V_p of the dye distribution by the following method. We introduce the closed curve, made of the straight lines that join the centers of boxes 1 to 4 and approaching the trajectory described by the

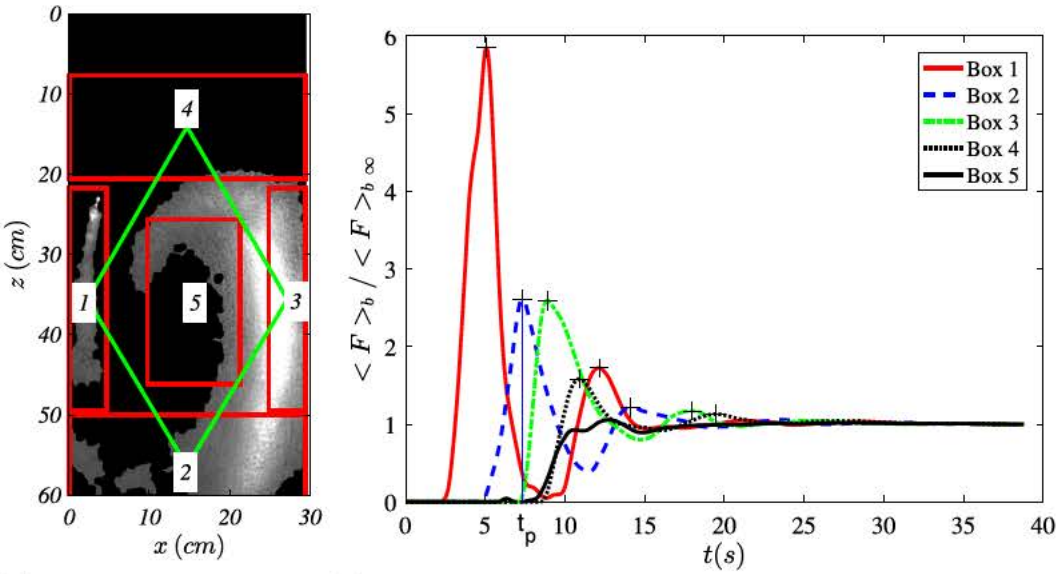

(a) Location of the five boxes.

(b) Temporal evolution of the gray levels averaged over each box

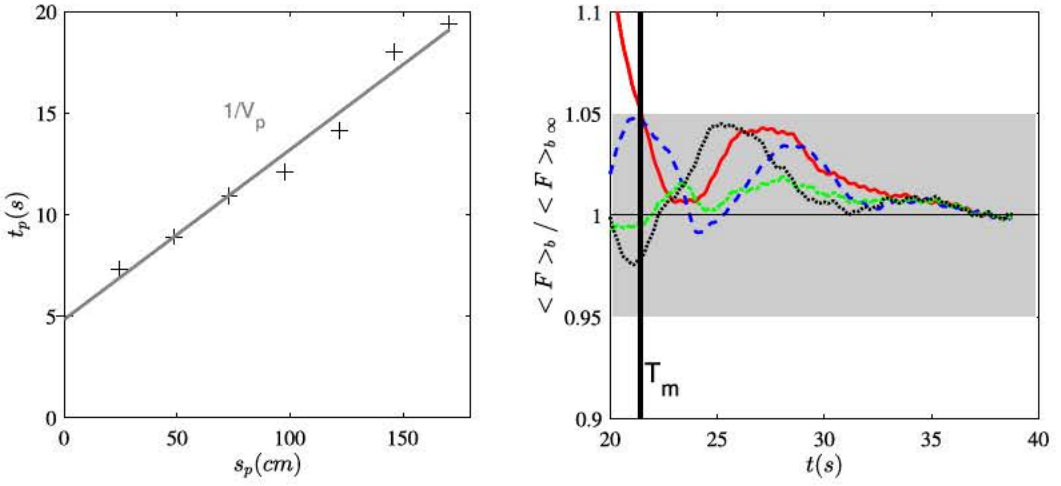

(c) Determination of the propagation velocity V_p

(d) Determination of the mixing time T_m

Fig. 8. Macroscopic characterisation of mixing. Configuration I2, injection point in the upstream leg.

dye (in green in Fig. 8(a)). Then, we consider the curvilinear abscissa s_p along this curve, which is oriented in the direction of the recirculating flow. Finally, the instants t_p are plotted in Fig. 8 (c) as a function of s_p. It turns out that t_p evolves linearly with s_p, which allows us to define the propagation velocity of the dye dis tribution as $V_p \quad ds_p/dt_p$. Concerning the mixing time T_m, it is defined as the time when the normalized grey levels of all the five boxes have reached the final value within ±5%. A zoom in of the normalized grey levels in each boxes are plotted as a function of time in Fig. 8(d). In this case, the mixing time is found equal to 21.4 s. Note that the present definition of T_m is consistent with that used in the determination of the mixing time in the homogeneous cases H1 2 by means of the colorimetry method.

Table 1 presents the propagation velocity V_p and the mixing time T_m averaged over the different runs for the five configurations. We can see that the propagation velocity of the dye distribution is close to the liquid mean velocity U for configurations H1 2 and I1 2, meaning that the advection of the dye distribution is produced by the mean liquid flow. The propagation velocity V_p can thus be used as an estimate of the liquid recirculation velocity, especially for the configuration I3 where no local measurement were per formed. In heterogeneous cases, the advection of the dye is domi nant in the vertical direction, both in the upstream and in the downstream legs, allowing to transport the dye over twice the height H of water during a turn over time of the recirculation.. A characteristic time T_a of advection of the dye can thus be defined from the propagation velocity (Table 2): $T_a \quad 2H/V_p$. In all hetero geneous cases I1 3, the advection time is found to be much smaller than the mixing time (Table 2), which confirms that the advection of the dye by the mean liquid flow is not the limiting mixing mechanism.

The characteristic time T_d of the mixing induced by the bubbles in direction i can thus be defined from the effective coefficient of diffusion D_i measured in a homogeneous bubble column (Alméras et al., 2015) as $T_d \quad \frac{l^2}{D_{ii}}$, where l is the length over which the diffusion occurs. In homogeneous cases H1 2 (Fig. 4), the diffu

Table 2
Decomposition of the mixing mechanisms. V_p: propagation velocity of the concentration field. D_h (resp. D_v): diffusion coefficient of the bubble-induced agitation in the horizontal direction (resp. vertical direction) measured in a homogeneous bubble column by Alméras et al. (2015). T_a $\frac{2H}{V_p}$: advection time. T_d: diffusion time with T_d $\frac{(H/2)^2}{D_v}$ in configurations H1-2 and T_d $\frac{(L/4)^2}{D_h}$ in configurations I1-3. T_m: experimental mixing time

	Advection		Diffusion			Exp.
	V_p cm/s	T_a s	D_h cm^2/s	D_v cm^2/s	T_d s	T_m s
H1	0	∞	2.5	5.1	300	139.3
H2	0	∞	2.6	5.9	270	126.5
I1	6.6	18.2	2.2	3.7	25.6	30.5
I2	12.2	9.8	2.4	4.6	23.4	21.5
I3	14.5	8.2	2.4	4.6	23.4	14.5

sion induced by the bubbles plays a role both in the vertical and horizontal direction. Even if the diffusion coefficient in the vertical direction is larger than the diffusion coefficient in the horizontal direction ($D_h > D_v$), the height of the column is much larger than its horizontal dimension. The diffusion time is thus controlled by the diffusion in the vertical direction. Since the dye is injected at mid height, the characteristic length is l $H/2$ and the diffusion time writes T_d $(H/2)^2/D_v$. In heterogeneous cases I1 3, the diffu sion by the bubble induced agitation is responsible for the mixing in the horizontal direction over the width $L/2$ of each leg of the recirculation. Since the diffusion acts simultaneously in the two opposite directions, the characteristic length of diffusion is l $L/4$ and the diffusion time writes T_d $(L/4)^2/D_h$.

Table 2 items the characteristic times of diffusion for the five configurations. For the homogeneous cases H1 2, even if the char acteristic time of diffusion is of the order of the mixing time, T_d remains more than twice T_m. This is probably related to the pres ence of the walls, in the vicinity of which a mean liquid velocity is present. The advection related to these liquid flow only plays a significant role once the dye distribution reaches the walls but is not negligible compared to the diffusion by bubble induced agita tion when looking at longer time. Even in the homogenous flow regime, the prediction of the mixing time in a bubble column can therefore not be accurately predicted by accounting only for the diffusion process that occurs in the absence of walls.

For the heterogeneous cases I1 2, the characteristic time of dif fusion is a remarkably good estimation of the measured mixing time. This means that the mixing of the dye caused by the bubble induced agitation in the horizontal direction is not affected by the large scale liquid flow and is well described by the diffusion coefficients measured in a homogeneous bubbly flow without walls effect (Alméras et al., 2015).

In contrast, the mixing time measured in case I3 is shorter than the diffusion time. It is visible in Fig. 7 that the steady recirculation loop is no longer stable and that large scale fluctuations of a dozen centimeter develop and cause a transport of the dye in the horizon tal direction between the upward and downward legs of the liquid recirculation. In this case, mixing results thus from a combined effect of both the advection by these large scales and by the agita tion induced by the bubbles. It is likely that, in this situation, mix ing can still be modeled similarly to the cases I1 2, but a quantitative prediction of the mixing time would require a com plete description of the large scales of the liquid velocity field. However, if the flow inhomogeneity would be increased, shear induced turbulence would develop at smaller length scales and its contribution to the mixing should be accounted for too.

Altogether, theses results suggest that the transport of a passive scalar within a bubbly flow can be modelled by an advection diffusion equation that accounts for the transport by the mean liq uid flow and the diffusion by the fluctuations. Regarding advection, we would like to stress the role of the mean flow that is generated close to the boundaries: even in a homogeneous bubble column there is a deficit of gas volume fraction over a distance $d/2$ to any vertical wall which generates a mean downward flow. Regard ing diffusion, as long as no shear induced turbulence is generated, it does not matter whether the flow is homogeneous or not: the diffusion coefficient is similar to that measured in a homogeneous bubble column, where only bubble induced agitation is present. At variance, when shear induced turbulence is present, in addition to the diffusion coefficient resulting from bubble induced agitation, a diffusion coefficient of the form D_t ν_t/Sc_t, where ν_t is the turbu lent viscosity and $Sc_t \approx 1$ has to be considered as proposed by Alméras et al. (2016).

5. Conclusion

The mixing of a passive scalar in a bubble column has been investigated experimentally either in the absence or in the pres ence of a large scale fluid recirculation in order to understand the impact of large scale buoyancy driven flow upon the mixing. Five configurations were studied, two cases corresponding to a homogeneous bubbly flow (H1 2) and three cases showing a large scale recirculation produced by an imposed horizontal gradi ent of gas volume fraction at the bottom of the column (I1 3). The time evolution of the dye within the column has been investigated by means of optical techniques, which allow to measure the prop agation velocity of the dye patch and the overall mixing time T_m. The propagation velocity turns out to be equal to the mean liquid circulation velocity independently of the configuration while the mixing time varies according to the configuration. Two character istic time scale are introduced: T_a, which characterizes the advec tion by the large scales and T_d, which characterizes the diffusion by the bubble induced agitation. The comparison between T_m and these two time scales leads to the following important conclusions.

In a homogeneous bubble column, the measured mixing time is of the order of the time predicted by considering only the diffusion by bubble induced agitation in an unbounded domain, but still sig nificantly smaller. The reason probably lies in the fact that mean liquid flows exist near the boundaries, either at the tank walls or on the dye injector in the middle of the column. Even if these flows are localized in a small volume of the column, their velocity scale is of the order of the bubble rising velocity ($\approx 3 \times 10^{-1}$ m/s), which is much larger than the transport velocity of the dye by diffusion at the scale of the column ($D_v/H \approx 5 \times 10^{-2}$ m/s). In practical situa tions, advection by mean flows can therefore hardly be neglected in the estimation of the mixing time, especially in a homogeneous bubble column.

In the presence of a large scale motion, the mixing time is con siderably reduced. In the case of a stable single loop recirculating flow (cases I1 2), the advection by the mean flow only acts in the vertical direction and the mixing time turns out to correspond to the time required for diffusion to transport the dye over one fourth of the column width. This allows to conclude that the diffusion

coefficients measured in an unbounded homogeneous bubble column are still valid in the presence of a large scale flow. When the inhomogeneity of the gas volume fraction becomes larger (case I3), large scale liquid motions of a dozen centimeter develop in the horizontal direction too, leading in a decrease of the mixing time. A reliable prediction of the advection by these large scales is then required to get a robust estimate of the mixing time.

Altogether these results indicate that, provided the shear induced turbulence produced by the buoyancy driven flow involves only scales larger than at least few bubble diameters, the mixing coefficients measured in an unbounded homogeneous bubbly flow are still relevant. The evolution of the concentration of a passive scalar in such a configuration is therefore the result of the advection by the large flow scales and the mixing by bubble induced agitation at small scales. In more heterogeneous cases, in which buoyancy driven flows generate shear induced turbulence involving scales smaller than the bubble, the diffusion coefficients should account for both bubble induced agitation and shear induced turbulence as shown in Alméras et al. (2016).

References

Abbas, M., Billet, A.-M., Roig, V., 2009. Experiments on mass transfer and mixing in a homogeneous bubbly flow. Turbul., Heat Mass Transf. Conf. 6.

Alméras, E., Plais, C., Euzenat, F., Risso, F., Roig, V., Augier, F., 2016. Scalar mixing in bubbly flows: experimental investigation and diffusivity modelling. Chem. Eng. Sci. 140, 114–122.

Alméras, E., Risso, F., Roig, V., Cazin, S., Plais, C., Augier, F., 2015. Mixing by bubble-induced turbulence. J. Fluid Mech. 776, 458–474.

Chaumat, H., Billet, A.-M., Delmas, H., 2006. Axial and radial investigation of hydrodynamics in a bubble column; influence of fluids flow rates and sparger type. Int. J. Chem. React. Eng. 4 (1).

Chen, R.C., Reese, J., Fan, L.-S., 1994. Flow structure in a three-dimensional bubble column and three-phase fluidized bed. AIChE J. 40 (7), 1093–1104.

Colombet, D., Legendre, D., Risso, F., Cockx, A., Guiraud, P., 2014. Dynamics and mass transfer of rising bubbles in a homogenous swarm at large gas volume fraction. J. Fluid Mech. 763, 254–285.

Combest, D.P., Ramachandran, P.A., Dudukovic, M.P., 2011. On the gradient diffusion hypothesis and passive scalar transport in turbulent flows. Ind. Eng. Chem. Res. 50, 8817–8823.

Degaleesan, S., Dudukovic, M., Pan, Y., 2001. Experimental study of gas-induced liquid-flow structures in bubble columns. AIChE J. 47 (9), 1913–1931.

Gabelle, J., Augier, F., Carvalho, A., Rousset, R., Morchain, J., 2011. Effect of tank size on kLa and mixing time in aerated stirred reactors with non-newtonian fluids. Can. J. Chem. Eng. 89, 1139–1153.

Kantarcia, N., Borakb, F., Ulgen, K.O., 2004. Bubble column reactors. Process Biochem. 40, 2263–2283.

Loisy, A., 2016. Direct numerical simulation of bubbly flows: coupling with scalar transport and turbulence. PhD thesis, Université de Lyon.

Mareuge, I., Lance, M., 1995. Bubble induced dispersion of a passive scalar in a bubbly flow. In: Int. Conf. on Multiphase Flow.

Martínez-Mercado, J., Chehata Gómez, D., Van Gils, D., Sun, C., Lohse, D., 2010. On bubble clustering and energy spectra in pseudo-turbulence. J. Fluid Mech. 650, 287–306.

Martínez-Mercado, J., Palacios-Morales, C., Zenit, R., 2007. Measurement of pseudoturbulence intensity in monodispersed bubbly liquids for $10 \leqslant re \leqslant 500$. Phys. Fluids 19, 103302.

Maximiano, P., 2015. Analysis and modelization of local hydrodynamics in bubble columns. PhD thesis, Chemical and Process Engineering. Université Grenoble Alpes.

McClure, D.D., Aboudha, N., Kavanagh, J.M., Fletcher, D.F., Barton, G.W., 2015. Mixing in bubble column reactors: experimental study and CFD modeling. Chem. Eng. J. 264, 291–301.

Mendez-Diaz, J., Serrano-García, J., Zenit, R., 2013. Power spectral distributions of pseudo-turbulent bubbly flows. Phys. Fluids 25, 043303.

Pandit, A., Joshi, J., 1983. Mixing in mechanically agitated gas-liquid contactors, bubble columns and modified bubble columns. Chem. Eng. J. 38, 1189–1215.

Plais, C., Augier, F., 2016. Effect of liquid viscosity on mixing time in bubble columns. Theoret. Found. Chem. Eng. 50, 969–974.

Riboux, G., Risso, F., Legendre, D., 2010. Experimental characterization of the agitation generated by bubbles rising at high Reynolds number. J. Fluid Mech. 643, 509–539.